JOURNAL OF APPLIED PHYSICS **114**, 213703 (2013)

Barrier height estimation of asymmetric metal-insulator-metal tunneling diodes

E. William Cowell III,[1] Sean W. Muir,[2] Douglas A. Keszler,[2] and John F. Wager[1]
[1]*School of Electrical Engineering and Computer Science, 1148 Kelley Engineering Center, Oregon State University, Corvallis, Oregon 97331-5501, USA*
[2]*Department of Chemistry, 153 Gilbert Hall, Oregon State University, Corvallis, Oregon 97331-4003, USA*

(Received 24 September 2013; accepted 17 November 2013; published online 5 December 2013)

A method is developed to estimate barrier heights of an asymmetric metal-insulator-metal (MIM) diode exhibiting Fowler-Nordheim tunneling. The method requires determination of slopes and intercepts of a $\log\left(\left|\frac{I}{(V+\Delta\phi)^2}\right|\right)$ versus $\frac{1}{V+\Delta\phi}$ plot rather than a $\log\left(\left|\frac{I}{(V)^2}\right|\right)$ versus $\frac{1}{V}$ plot (i.e., a conventional Fowler-Nordheim plot), where I, V, and $\Delta\phi$ refer to tunneling current, applied voltage, and the difference in barrier heights, respectively. As the value of $\Delta\phi$ directly impacts the applied electric field magnitude, it is a critical component in barrier height determination from a current-voltage measurement. Conventional Fowler-Nordheim plot analysis does not employ $\Delta\phi$, which compromises the accuracy of barrier height estimation when $\Delta\phi \neq 0$. Using the described method, the barrier heights of a ZrCuNiAl/Al_2O_3/Al MIM diode are estimated to be 1.75 V and 1.07 V, respectively, and the Al_2O_3 tunneling effective mass is estimated to be 0.47. Additional MIM diodes are analyzed to show that the accuracy of MIM diode barrier height and effective mass estimates is highly sensitive to contamination and/or energy imparted during the deposition of the upper electrode. © *2013 AIP Publishing LLC*. [http://dx.doi.org/10.1063/1.4839695]

I. INTRODUCTION

Electron emission from a metal surface into vacuum (Fig. 1(a)) is modeled using Fowler-Nordheim tunneling theory.[1] Emission current, I, is described by

$$I = \frac{AV^2}{s\phi_b}\exp\left(\frac{-Bs(\phi_b)^{\frac{3}{2}}}{V}\right), \tag{1}$$

where A and B are constants, V is the applied voltage driving electron emission, s is the distance between the metal surface, and the point at which a voltage is applied, i.e., thickness of the barrier, and ϕ_b is the barrier height. Note that Fowler and Nordheim conclude that inclusion of image force barrier rounding is not necessary at high fields and ordinary temperatures as the image force effect is small relative to the barrier height required for tunneling. It is also important to note, as illustrated in Fig. 1(a), that there is only one barrier to electron emission in the original description of Fowler-Nordheim tunneling. The field driving electron emission is applied between the Fermi level of the metal surface and the vacuum level. Equation (1) predicts a linear relationship between $\log(\frac{I}{V^2})$ and $\frac{1}{V}$, as first described by Millikan and Laruitsen.[2] A plot of $\log(\frac{I}{V^2})$ versus $\frac{1}{V}$ is referred to as a Fowler-Nordheim plot. If a Fowler-Nordheim plot can be accurately fit to experimental emission current data, ϕ_b can be estimated as a fit parameter using accepted values of A and B. Electron emission is into vacuum, so the mass of a tunneling electron is assumed to be equal to the electron rest mass.

Simmons[3,4] extends the theory of Fowler-Nordheim tunneling to a metal-insulator-metal (MIM) thin-film structure, where electrons tunnel through an insulator located between two metal electrodes. Tunneling current can be modeled using either an ideal trapezoidal barrier (Fig. 1(b)) or a barrier of arbitrary shape. In the context of this contribution, this structure is referred to as a MIM diode. Conducting electrons in a MIM diode encounter two barriers, ϕ_{b1} and ϕ_{b2}. When MIM diode barrier heights are not identical, the Fowler-Nordheim tunneling currents are asymmetrical with respect to applied voltage polarity. The resulting current-voltage relationship is given as

$$I = \frac{A(V+\Delta\phi)^2}{s\phi_b}\exp\left(\frac{-Bs(\phi_b)^{\frac{3}{2}}}{V+\Delta\phi}\right), \tag{2}$$

where $\Delta\phi = \phi_{b1} - \phi_{b2}$ is the difference in barrier heights. The only difference between Eqs. (1) and (2) is the inclusion of $\Delta\phi$.

Equation (2) predicts a linear relationship between $\log\left(\left|\frac{I}{(V+\Delta\phi)^2}\right|\right)$ versus $\frac{1}{V+\Delta\phi}$. If such a plot can be accurately fit to experimental MIM diode current-voltage data, ϕ_{b1} and ϕ_{b2} can be estimated as fitting parameters. However, to accomplish this, $\Delta\phi$ must first be assessed. Thus, a distinguishing feature of the barrier height assessment procedure described herein is the recognition of the importance of accounting for $\Delta\phi$. Fowler-Nordheim modeling is typically based on Eq. (1), which assumes $\Delta\phi = 0$.[5–7] MIM diodes fabricated with differing electrode materials have different barrier heights and should not be modeled with the assumption that $\Delta\phi = 0$.

In addition to accounting for $\Delta\phi$ in our assessment of MIM diode barrier heights, use of an amorphous metal thin film (AMTF) lower electrode is of critical importance in accomplishing the work reported herein. An AMTF possesses

 © 2013 AIP Publishing LLC

[This article is copyrighted as indicated in the article. Reuse of AIP content is subject to the terms at: http://scitation.aip.org/termsconditions. Downloaded to] IP: 128.193.163.187 On: Mon, 10 Mar 2014 19:05:15

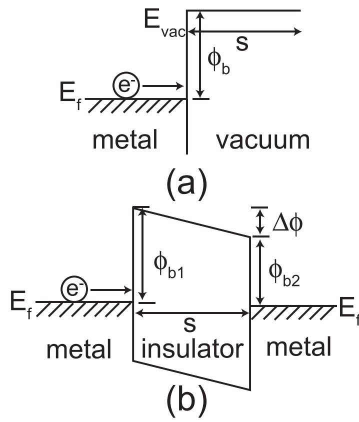

FIG. 1. (a) Equilibrium energy band diagram of a metal surface in a vacuum as presented by Fowler and Nordheim.[1] (b) Equilibrium energy band diagram of two metal electrodes separated by a thin insulating film as presented by Simmons.[4]

an ultra-smooth surface with surface roughness less than 0.2 nm,[8,9] facilitating fabrication of a MIM diode in which the electric field is sufficiently uniform that its current-voltage characteristics are accurately described by Fowler-Nordheim tunneling theory, as modified by Simmons, over multiple decades of current.[8] In this contribution, we describe a method to assess barrier heights of MIM diodes fabricated with AMTF lower electrodes. Estimates for $\Delta\phi$ and the two interfacial barrier heights, ϕ_{b1} and ϕ_{b2}, are computed. The use of an assumed barrier thickness, equal to the thickness of the deposited insulator, allows the estimation of a tunneling electron's effective mass.

II. EXPERIMENT

Amorphous metal thin films were deposited from 3-in. vacuum-arc-melted multi-component metal targets purchased from Kamis Inc. with stoichiometric compositions of $Zr_{40}Cu_{35}Al_{15}Ni_{10}$ and $Ti_{25}Al_{75}$. ZrCuAlNi films were deposited via DC magnetron sputtering at a power of 60 W, a pressure of 3 mTorr, and a 20 sccm flow of Ar gas. TiAl films were deposited via DC magnetron sputtering at a power of 90 W, a pressure of 3 mTorr, and a 20 sccm flow of Ar gas. Thin-film thicknesses were targeted at 200 nm.

Al_2O_3 films were deposited via atomic layer deposition (ALD). The ZrCuAlNi diodes had 10 nm of Al_2O_3 deposited in a Picosun SUNALE R-150B ALD reactor using trimethylaluminum (TMA) and de-ionized water at a temperature of 300 °C. De-ionized water and TMA pulse times of 0.1 s were used with a 2 s purge time between pulses. The TiAl diode had 10 nm of Al_2O_3 deposited in a Beneq P400 ALD reactor using TMA and de-ionized water at a temperature of 300 °C. TMA pulses of 0.2 s and deionized water pulses of 0.3 s were used with a 2.2 s purge between pulses.

MIM diode structures were completed by depositing top contacts through a shadow mask with 1.1 mm^2 circular openings, creating device areas near 1 mm^2. The ZrCuAlNi diodes had Al top contacts deposited via thermal evaporation, DC magnetron sputtering, or electron beam deposition. DC magnetron sputter deposition of Al was carried out at a power of 60 W, a pressure of 3 mTorr, and a 20 sccm flow of Ar gas. Electron-beam deposition of Al was performed using a Temescal 2CK Super Source electron-gun along with a CV8 electron beam power supply at 53% of full current. The TiAl diode had TiAl top contacts deposited via DC magnetron sputtering at a power of 90 W and a pressure of 3 mTorr of pressure, using a 20 sccm flow of Ar gas.

Electrical measurements were performed with a Hewlett-Packard 4156 C semiconductor parameter analyzer. The blanket lower ZrCuAlNi and TiAl electrodes were held at ground potential with bias applied to the upper electrodes. The magnitude of the applied voltage bias was scaled to target maximum current levels in the μA range.

III. EXPERIMENTAL RESULTS AND DISCUSSION

A. Barrier height estimation

Energy band diagrams illustrate the importance of $\Delta\phi$ in the modeling of tunneling currents for a MIM diode. Figures 2(a) and 2(b) present the physical structure and equilibrium energy band diagram, respectively, of an asymmetric tunneling MIM diode (M1 $\neq$ M2). The lower electrode (M1) is considered to be grounded, while a voltage is applied to the upper electrode (M2). Figure 2(c) presents a non-equilibrium energy band diagram of a tunneling MIM diode with a positive applied voltage, V^+. The current generated by application of a positive voltage of magnitude greater than the collecting barrier height ϕ_{b2} is given by[4]

$$I^+ = \frac{(Area)C_1}{\phi_{b1}}\frac{(V+\Delta\phi)^2}{s^2}\exp\left(-C_2\sqrt{m^*}(\phi_{b1})^{\frac{3}{2}}\frac{s}{V+\Delta\phi}\right), \tag{3}$$

where $(Area)$ is the device area, ϕ_{b1} is the height of the injecting barrier formed between electrode M1 and the insulator, s is the thickness of the barrier, and m^* is the tunneling effective mass of an electron in the insulator. $\Delta\phi$ is the difference between the two barrier heights, defined with the convention

$$\Delta\phi = \phi_{b1} - \phi_{b2}. \tag{4}$$

C_1 is equal to[4]

$$C_1 = \frac{2.2q^2}{8\pi h} = 3.4\times10^{-6}\frac{A}{V}, \tag{5}$$

where q is the charge of an electron and h is Planck's constant. C_2 is defined as[4]

$$C_2 = \frac{23\pi\sqrt{qm_0}}{6h} = 6.9\times10^9\frac{1}{m\sqrt{V}}, \tag{6}$$

where m_0 is the electron rest mass. As defined, both C_1 and C_2 are comprised entirely of universal constants, and are not related to material properties of the MIM components. From Eq. (3), the positive current, I^+, depends on the barrier height of the injecting barrier, ϕ_{b1}, and the height of the collecting barrier, ϕ_{b2}, through the $\Delta\phi$ terms.

[This article is copyrighted as indicated in the article. Reuse of AIP content is subject to the terms at: http://scitation.aip.org/termsconditions. Downloaded to] IP: 128.193.163.187 On: Mon, 10 Mar 2014 19:05:15

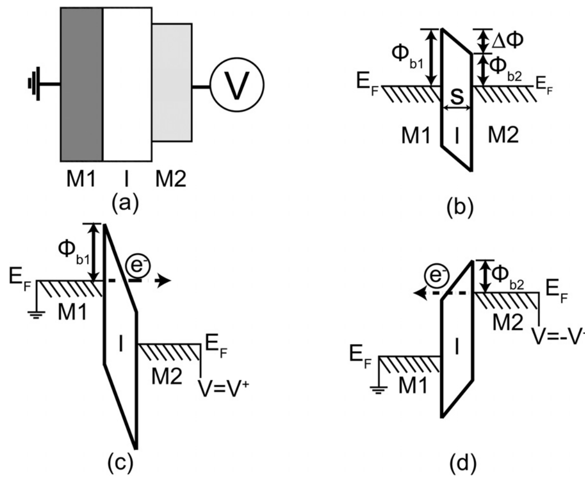

FIG. 2. (a) Illustration of the physical layers of an asymmetric tunneling MIM diode. M1 is a blanket lower electrode, I is an insulator, and M2 is a shadow mask deposited upper electrode. (b) Equilibrium energy band diagram of an asymmetric tunneling MIM diode. (c) Non-equilibrium energy band diagram of an asymmetric tunneling MIM diode at a positive applied bias. (d) Non-equilibrium energy band diagram of an asymmetric tunneling MIM diode at a negative applied bias.

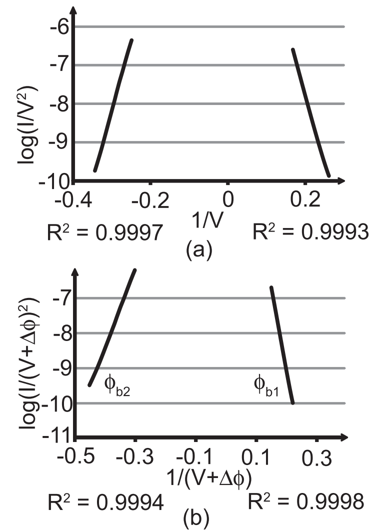

FIG. 3. (a) A Fowler-Nordheim plot of a ZrCuAlNi/Al_2O_3/Al tunneling MIM diode, i.e., $\log\left(\left|\frac{I}{V^2}\right|\right)$ versus $\frac{1}{V}$. (b) A plot of $\log\left(\left|\frac{I}{(V+\Delta\phi)^2}\right|\right)$ vs. $\frac{1}{V+\Delta\phi}$. Coefficient of determination (R^2) values for linear-least-squares-fits of the presented data at positive and negative polarities are included below the plots.

Figure 2(d) presents a non-equilibrium energy band diagram of a tunneling MIM diode with a negative applied voltage, $V < 0$. The current generated by the application of a negative voltage of magnitude greater than the collecting barrier height ϕ_{b1} is given by[4]

$$I^- = \frac{-(Area)C_1}{\phi_{b2}}\frac{(V+\Delta\phi)^2}{s^2}\exp\left(C_2\sqrt{m^*}(\phi_{b2})^{\frac{3}{2}}\frac{s}{V+\Delta\phi}\right), \tag{7}$$

where ϕ_{b2} is the height of the injecting barrier formed between the insulator and electrode M2. Equation (7) shows that I^- depends on the injecting barrier height, ϕ_{b2}, and on the collecting barrier height, ϕ_{b1}, through $\Delta\phi$. Equations (3) and (7) illustrate that a difference in barrier heights, resulting in a non-zero value of $\Delta\phi$, is the source of asymmetry for a tunneling MIM diode. To accurately assess tunneling conduction for a MIM diode, $\Delta\phi$ must be determined and included in the modeling.

A plot of the $\log(\frac{I}{V^2})$ versus $\frac{1}{V}$, i.e., a Fowler-Nordheim plot, produces a straight line when the applied voltage is greater than the height of the injecting barrier, i.e., ϕ_{b1} for positive applied voltages and ϕ_{b2} for negative applied voltages, and the conduction mechanism of the measured device is dominated by Fowler-Nordheim tunneling. Figure 3(a) presents a Fowler-Nordheim plot for a MIM diode fabricated with a 200 nm thick amorphous ZrCuAlNi lower electrode, a 10 nm Al_2O_3 insulator, and a thermally evaporated Al upper electrode. Linear behavior is observed over more than three decades of current magnitude. The lower limit of the current data is defined by the noise floor of the electrical measurement system (approximately 3 nA), which is related to the displacement current associated with the applied voltage sweep rate. The coefficient of determination values (R^2) of both fits, shown below the plots, indicate the excellent quality of the fit between the measured data and the model. An R^2 value greater than 0.99 indicates the dominance of Fowler-Nordheim tunneling.

Although Fowler-Nordheim plots such as shown in Fig. 3(a) have been extensively used in prior assessments, they are inappropriate for careful analysis of an asymmetric MIM diode since the effect of $\Delta\phi$ has been ignored. To facilitate evaluation of barrier heights, i.e., ϕ_{b1}, ϕ_{b2}, or $\Delta\phi$, Eq. (3) is linearized as

$$\log\left(\frac{I^+}{(V+\Delta\phi)^2}\right) = \frac{-C_2 s\sqrt{m^*}(\phi_{b1})^{\frac{3}{2}}}{2.3}\frac{1}{V+\Delta\phi} + \log\left(\frac{(Area)C_1}{s^2\phi_{b1}}\right), \tag{8}$$

and Eq. (7) is linearized as

$$\log\left(\left|\frac{I^-}{(V+\Delta\phi)^2}\right|\right) = \frac{-C_2 s\sqrt{m^*}(\phi_{b2})^{\frac{3}{2}}}{2.3}\frac{1}{V+\Delta\phi} + \log\left(\frac{(Area)C_1}{s^2\phi_{b2}}\right). \tag{9}$$

Equations (8) and (9) demonstrate that a linear relationship exists between $\log\left(\left|\frac{I}{(V+\Delta\phi)^2}\right|\right)$ and $\frac{1}{V+\Delta\phi}$ for MIM tunneling diode.

Figure 3(b) presents the data illustrated in Fig. 3(a) replotted using Eqs. (8) and (9). A comparison of the slopes presented in Figs. 3(a) and 3(b) reveals that the addition of $\Delta\phi$ into the linearized I–V data has increased the difference in slopes observed between voltage polarities. The R^2 values shown in Figs. 3(a) and 3(b) are greater than 0.99, confirming Fowler-Nordheim tunneling as the dominant conduction mechanism and also that either set of equations (i.e., Eqs. (1) or (8) or (9)) can be used to obtain an excellent fit to the data. However, the impact of $\Delta\phi$ on the slope of a

[This article is copyrighted as indicated in the article. Reuse of AIP content is subject to the terms at: http://scitation.aip.org/termsconditions. Downloaded to] IP: 128.193.163.187 On: Mon, 10 Mar 2014 19:05:15

Fowler-Nordheim plot suggests that modeling of asymmetric MIM diode I–V characteristics should include $\Delta\phi$, as suggested by Simmons.

Using Simmons' theory and measured MIM tunneling diode I–V characteristics enables assessment of barrier heights and related parameters. The values of $\Delta\phi$, ϕ_{b1}, and ϕ_{b2} are determined through iterative assessment of I–V data by linear-least-squares-fits to determine slopes and intercepts as described next.

The slope magnitude and intercept of I^+, linearized according to Eq. (8), are described, respectively, as

$$m^+ = \frac{-C_2 s\sqrt{m^*}(\phi_{b1})^{\frac{3}{2}}}{2.3}, \tag{10}$$

and

$$b^+ = \log\left(\frac{(Area)C_1}{s^2\phi_{b1}}\right). \tag{11}$$

The slope magnitude and intercept of I^-, linearized according to Eq. (9), are given, respectively, by

$$m^- = \frac{C_2 s\sqrt{m^*}(\phi_{b2})^{\frac{3}{2}}}{2.3}, \tag{12}$$

and

$$b^- = \log\left(\frac{(Area)C_1}{s^2\phi_{b2}}\right). \tag{13}$$

The signs of the slope magnitudes, m^- and m^+, are opposite due to the difference in signs of the applied voltages in Eqs. (8) and (9). The barrier-height ratio from the linear-least-squares-fit slopes defined in Eqs. (10) and (12) is given by

$$\frac{\phi_{b1}}{\phi_{b2}} = \left(\left|\frac{m^+}{m^-}\right|\right)^{\frac{2}{3}} = r. \tag{14}$$

Equation (14) assumes that the effective mass, m*, and the barrier thickness, s, are equivalent for both applied voltage polarities. Assuming this equivalence and the equivalence of diode area for both voltage polarities, the barrier-height ratio from the linear-least-squares-fit intercepts defined in Eqs. (11) and (13) is given by

$$\frac{\phi_{b1}}{\phi_{b2}} = 10^{b^- - b^+} = r. \tag{15}$$

Given this background, iterative assessment of $\Delta\phi$ proceeds as follows. I^+ and I^- experimental data are plotted in accordance with Eqs. (8) and (9), respectively, giving rise to plots such as the one shown in Fig. 3(b). However, accurate assessments of Eqs. (8) and (9) require that $\Delta\phi$ is known, which it is not (yet). Thus, an initial guess for $\Delta\phi$ is made. This value of $\Delta\phi$ is used to evaluate Eqs. (8) and (9), and the resulting estimates of m^+, b^+, m^-, and b^- are obtained by linear regression of data plotted in the format shown in Fig. 3(b). The viability of this initial estimate of $\Delta\phi$ is tested by evaluating Eq. (14) using m^+ and m^-, and Eq. (15) using b^+ and b^-, and assessing whether or not Eqs. (14) and (15) are equal to one another. If Eqs. (14) and (15) are not equal, this procedure is iterated with new values of $\Delta\phi$ until Eqs. (14) and (15) are equal and an optimal estimate of $\Delta\phi$ is obtained.

Once an optimum value of $\Delta\phi$ is established, both barrier heights are determined using either Eqs. (14) or (15) and

$$\Delta\phi = \phi_{b1} - \phi_{b2}. \tag{16}$$

More precisely, the barrier heights are uniquely determined to be

$$\phi_{b1} = \frac{r\Delta\phi}{r-1}, \tag{17}$$

and

$$\phi_{b2} = \frac{\Delta\phi}{r-1}, \tag{18}$$

where r is the ratio determined by Eq. (14) or (15). Furthermore, the effective mass of a tunneling electron may be calculated from Eq. (10) or (12) with an estimated barrier thickness, s, yielding

$$m^* = \left(\frac{2.3m^+}{-C_2 s(\phi_{b1})^{\frac{3}{2}}}\right)^2 = \left(\frac{2.3m^-}{C_2 s(\phi_{b2})^{\frac{3}{2}}}\right)^2. \tag{19}$$

This procedure is used to produce the data shown in Fig. 3(b), leading to the equilibrium band diagram shown in Fig. 4. This results in a $\Delta\phi$ estimate of 0.68 V, a ϕ_{b1} of 1.75 V, and a ϕ_{b2} of 1.07 V. Using an assumed upper aluminum electrode work function of 4.28 V,[10] the Al_2O_3 electron affinity is estimated to be 3.21 V. This value is slightly larger than those previously reported, i.e., 2.5, 2.8, and 2.7 V.[11–13] Using Eq. (19) with an estimated barrier thickness of 10 nm (equal to the ALD film thickness), the effective mass of an electron tunneling through Al_2O_3 is estimated to be 0.47. The effective mass a tunneling electron in thin-film Al_2O_3 has been reported to be 0.24[13] and 0.4.[14]

Two primary assumptions are made in the assessment leading to Fig. 4. First, image force rounding at the two

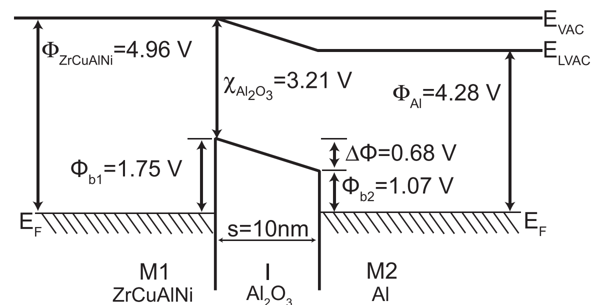

FIG. 4. An equilibrium energy band diagram of the tunneling MIM diode measured to produce the data presented in Fig. 3. The barrier heights, ϕ_{b1} and ϕ_{b2}, and the difference in barrier heights, $\Delta\phi$, are determined via barrier height ratio convergence.

[This article is copyrighted as indicated in the article. Reuse of AIP content is subject to the terms at: http://scitation.aip.org/termsconditions. Downloaded to] IP: 128.193.163.187 On: Mon, 10 Mar 2014 19:05:15

interfaces is ignored. Second, s is estimated to be equal to the thickness of the deposited insulator. Thus, the effects on s from electrode native oxides are ignored. While these factors undoubtedly contribute to the accuracy of our estimates, it is noteworthy that the ultra-smooth nature of the AMTF surface is essential for obtaining an I–V curve capable of being fit to Fowler-Nordheim tunneling theory to a precision in which $R^2 > 0.99$.

TABLE I. R^2 values of linearized $\log\left(\left|\frac{I}{(V+\Delta\phi)^2}\right|\right)$ vs $\frac{1}{V+\Delta\phi}$ for data of both voltage polarities, calculated barrier heights, and calculated material parameters of MIM diodes possessing Al upper electrodes fabricated with different deposition techniques.

Tool	R^2+	R^2-	$\Delta\phi$	ϕ_{b1}	ϕ_{b2}	m*	χ
Thermal1	0.999	0.9999	0.69	1.75	1.07	0.47	3.21
Thermal2	0.999	0.9999	0.46	1.55	1.09	0.71	3.19
Sputter	0.995	0.998	0.87	2.37	1.50	0.17	2.78
Ebeam	0.999	0.999	0.34	0.96	0.62	1.14	3.66

B. Barrier height estimation sensitivity

The upper Al electrode used in the MIM diode assessed in Fig. 4 is deposited by thermal evaporation using a relatively pristine, turbomechanically pumped deposition system. Thermal evaporation is a gentle deposition process that does not impart significant kinetic energy to a surface. Thus, we consider the estimates summarized in Fig. 4 to be our best appraisal of the intrinsic physical parameters of our ZrCuAlNi/Al_2O_3/Al MIM diode.

We next compare four ZrCuAlNi/Al_2O_3/Al MIM diodes fabricated as identically as possible except for the upper Al electrode deposition method. We find that the electrical characteristics of a MIM diode are extraordinarily sensitive to the method in which the upper Al electrode metal is deposited. Although we employ the same barrier height assessment method as used for the evaluation presented in Fig. 4, it is important to recognize that resulting estimates of $\Delta\phi$, ϕ_{b1}, ϕ_{b2}, and m* may to some extent be non-physical. Our hypothesis is that alternative deposition techniques likely introduce more contamination and/or deleterious deposition energy into the MIM diode insulator.

Two MIM diodes fabricated with concurrently deposited lower amorphous metal electrodes (200 nm ZrCuAlNi) and 10 nm ALD Al_2O_3 insulators were fabricated, ideally creating a common barrier height ϕ_{b1} for both diodes. Diode fabrication was completed by thermal evaporation of top Al electrodes in two different vacuum systems. Fowler-Nordheim plots of representative diodes, shown in Fig. 5(a), differ between the two vacuum systems. $\Delta\phi$ is not included in the plots as the optimum values of $\Delta\phi$ differ between the two diodes, creating different axes. R^2 values of linearized $\log\left(\left|\frac{I}{(V+\Delta\phi)^2}\right|\right)$ vs $\frac{1}{V+\Delta\phi}$ for the two diodes, shown in Table I, are >0.99 for both diodes, indicating excellent linear fits at the optimum $\Delta\phi$ values.

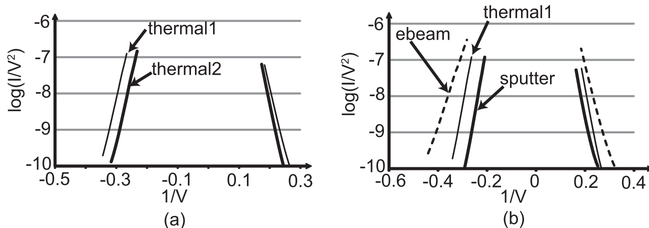

FIG. 5. (a) Fowler-Nordheim plots of two MIM diodes fabricated with concurrently deposited lower electrodes (ZrCuAlNi) and Al_2O_3 insulators. The diodes have thermally evaporated Al upper electrodes deposited in two different systems. (b) Fowler-Nordheim plots of three MIM diodes fabricated with concurrently deposited lower electrodes (ZrCuAlNi) and Al_2O_3 insulators. The diodes have Al upper electrodes deposited via thermal evaporation, DC magnetron sputtering, and electron beam deposition.

The barrier heights and material parameters determined through the linearization of I–V characteristics are summarized in Table I. The values of ϕ_{b2} and χ are equivalent, while the values of ϕ_{b1} and $\Delta\phi$ are different. m* values of the two diodes, calculated using Eq. (19), also differ, with the m* value of Thermal2, i.e., 0.71, being higher than reported values of effective mass in Al_2O_3, i.e., 0.24[13] and 0.4.[14] A conclusion drawn from the comparison of barrier heights and material parameters is that barrier heights of MIM diodes are readily modulated by the upper electrode deposition technique. These results are highly reproducible. The cause of the barrier height and material parameter differences in this case is attributed to the unique characteristics of the thermal evaporation systems used to deposit the Al upper electrodes. Thermal2 is a heavily used (non-pristine) system with a diffusion-pump-based vacuum system, while Thermal1 is a less-used (pristine) turbo-pumped system. The base pressure of Thermal1 is an order of magnitude lower than the base pressure of Thermal2, which results in a cleaner interface between the insulator and the upper electrode. The usage level of the tools likely contributes to a difference in contamination at the insulator/upper electrode interface.

Barrier height and material parameter differences are more pronounced between diodes with upper Al electrodes deposited by different techniques. Fowler-Nordheim plots for three MIM diodes are illustrated in Fig. 5(b). Lower AMTF electrodes (200 nm ZrCuAlNi) and 10-nm Al_2O_3 insulators were deposited concurrently, while upper Al electrodes were deposited by thermal evaporation, electron-beam evaporation, and sputtering. The thermal results represent those of the Thermal1 diode from Fig. 5(a). Once again, $\Delta\phi$ is not included in the plots as this would create differing axes for each of the three diodes. As presented in Table I, the R^2 values of all three diodes are >0.99 for positive and negative polarities at the optimum values of $\Delta\phi$, indicating excellent linear fits.

Barrier heights, i.e., $\Delta\phi$, ϕ_{b1}, and ϕ_{b2}, (Table I) differ among the three diodes. Deposition tool vacuum systems are all turbo-pumped, so a difference in interfacial contamination caused by the deposition tool vacuum system is not expected. The energetic interactions between the impinging Al and the Al_2O_3, modulating the chemistry associated with barrier formation, are the most likely cause of the barrier height and material parameter differences between the

[This article is copyrighted as indicated in the article. Reuse of AIP content is subject to the terms at: http://scitation.aip.org/termsconditions. Downloaded to] IP: 128.193.163.187 On: Mon, 10 Mar 2014 19:05:15

sputter and thermal depositions. The energy of deposited Al is greater in DC magnetron sputtering than thermal evaporation. The barrier heights of the sputtered diode, shown in Table I, are determined to be significantly higher than the barriers of the Thermal1 diode. The upper electrode deposition method is the only difference in the fabrication and testing of the devices. Therefore, the upper electrode deposition is almost certainly the cause of the barrier height parameter differences. The calculated values of the insulator electron affinity and electron effective mass for the sputtered diode, i.e., 2.78 eV, and 0.17, respectively, are close to reported values. This suggests that energy associated with the sputter deposition of Al drives interfacial chemistry enabling ideal Fowler-Nordheim tunneling through a trapezoidal barrier.

The electron-beam diode I–V characteristics differ significantly from the other diodes in both polarities. The process of electron-beam deposition is known to generate x-rays, which can cause damage to insulating films.[15] Both calculated barrier heights (ϕ_{b1} and ϕ_{b2}) of this diode, presented in Table I, are significantly lower than those of the other diodes. A significant change to the barrier heights is consistent with the hypothesis that the electron-beam deposition significantly damages the Al_2O_3 insulator. The calculated value of Al_2O_3 electron affinity is 3.66 eV, which is significantly higher than values reported in the literature as well as the electron affinity values calculated for the other three MIM diodes. The calculated value of the effective mass of a tunneling electron is 1.14 time the rest mass of an electron, considerably higher than observed for the other diodes. Reports of tunneling electron effective mass in SiO_2 are more prominent in the literature, with values ranging between 0.42 and 0.5.[16–19] Therefore, a calculated effective mass of 1.14 is a strong indication that the MIM diode with an electron-beam deposited Al upper electrode has non-ideal trapezoidal barrier and material parameter characteristics.

The method for characterization of diode parameters allows for the assessment of the effects of deposition on barrier height, electron affinity, and tunneling electron effective mass. It is important to note that all of the analyzed diodes possess linearized I–V characteristics with R^2 values greater than 0.99, which is expected for MIM diode currents dominated by Fowler-Nordheim conduction. The only difference between the four presented MIM diodes is the method used to deposit the upper Al electrodes. Therefore, differences in derived parameters suggest that the method of Al deposition significantly affects barrier heights and material parameters.

C. A MIM tunneling diode fabricated with symmetric electrode materials

The MIM tunneling diodes discussed to this point have been fabricated with different top and bottom electrodes. MIM diodes possessing ZrCuAlNi lower electrodes and Al upper electrodes are expected to exhibit asymmetric I–V characteristics because of the difference in work functions of the electrodes. Analysis of I–V characteristics from diodes fabricated with different Al deposition methods demonstrates that the work function of the electrodes and the chemistry associated with barrier formation must be considered. We next analyze a tunneling MIM diode fabricated with the same lower and upper electrode material to further illustrate that tunneling MIM diode I–V characteristics are strongly dependent on processing conditions.

Figure 6 presents the linearized I–V characteristics, estimated barrier heights, and estimated material parameters of a tunneling MIM diode fabricated with a TiAl AMTF lower electrode, a 10 nm Al_2O_3 insulator deposited via ALD, and a TiAl AMTF upper electrode. TiAl has been shown to be amorphous when deposited in thin-film form.[20,21] The presented R^2 values indicate excellent linear fits for data from both voltage polarities, suggesting Fowler-Nordheim tunneling is the dominant conduction mechanism. The estimated barrier heights, however, are not equivalent; the estimated value of $\Delta\phi$ is 0.19 V. An apparently symmetric device structure is producing asymmetric I–V characteristics. Using the upper electrode/insulator barrier (ϕ_{b2}) and a TiAl work function of 4.6 V (measured via ambient Kelvin Probe analysis), the electron affinity of Al_2O_3 is found to be 4.0 V. Using ϕ_{b2} in the insulator electron affinity calculation is consistent with the other calculations to this point, where an Al work-function of 4.28 eV was used. From the slopes of the linearized I–V data and an assumed tunneling barrier thickness of 10 nm, the effective mass of a tunneling electron is estimated to be 1.5. If barrier heights were determined exclusively by the materials used to fabricate a tunneling MIM diode, the estimated heights should be symmetric when both TiAl electrodes are deposited in exactly the same fashion. A non-zero value of $\Delta\phi$ and high values of Al_2O_3 electron affinity and tunneling electron effective mass confirm that the nature of the two $TiAl/Al_2O_3$ interfaces has a significant impact on the I–V characteristics of tunneling MIM diodes. The interfacial chemistry that occurs during the deposition of upper electrode material markedly differs from that of the lower electrode.

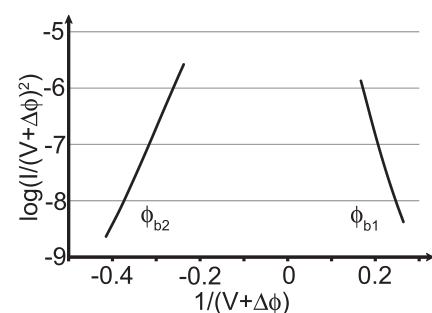

$y^- = 17.5x + 1.45$ $R^2 = 0.9993$ $y^+ = -26.1x + 1.57$ $R^2 = 0.9967$

(a)

ϕ_{b1} (V)	ϕ_{b2} (V)	$\Delta\phi$ (V)	χ (V)	m*
0.80	0.61	0.19	4.0	1.5

(b)

FIG. 6. (a) Current-voltage characteristics linearized at an optimum value of $\Delta\phi$ for a tunneling MIM diode fabricated with a TiAl AMTF lower electrode, a 10 nm Al_2O_3 insulator, and a TiAl AMTF upper electrode. (b) Calculated barrier heights and material parameters for the diode shown in (a).

[This article is copyrighted as indicated in the article. Reuse of AIP content is subject to the terms at: http://scitation.aip.org/termsconditions. Downloaded to] IP: 128.193.163.187 On: Mon, 10 Mar 2014 19:05:15

IV. CONCLUSIONS

A method for estimating barrier heights and the tunneling effective mass of a MIM diode exhibiting Fowler-Nordheim tunneling is described. Rather than employing a conventional Fowler-Nordheim plot of $\log\left(\left|\frac{I}{V^2}\right|\right)$ versus $\frac{1}{V}$, this assessment procedure requires that $\log\left(\left|\frac{I}{(V+\Delta\phi)^2}\right|\right)$ versus $\frac{1}{V+\Delta\phi}$ be plotted for both voltage polarities at an optimum value of $\Delta\phi$, i.e., the difference in barrier heights. The method for evaluation of an optimum value of $\Delta\phi$ is described, and is of critical importance to barrier height estimation. For a pristine ZrCuAlNi/Al_2O_3/Al; MIM diode, the barrier heights ϕ_{b1} and ϕ_{b2} are estimated to be 1.75 V and 1.07 V, respectively, and the tunneling effective mass is estimated to be 0.47. Contamination and/or an increase in the energy imparted during deposition of the upper Al electrode leads to different and less reliable barrier height and tunneling effective mass estimates since MIM diode tunneling current is extraordinarily sensitive to these effects.

ACKNOWLEDGMENTS

This material was based upon work supported by the National Science Foundation under Grant Nos. CHE-0847970 and CHE-1102637. The authors would like to thank Professor John Conley and Nasir Alimardani at Oregon State University for the ZrCuAlNi MIM diode Al_2O_3 ALD depositions, Ram Ravichandran at Oregon State University for the Al electron-beam deposition, and Chris Knutson and Wei Wang at Oregon State University for sharing their valuable insights regarding this research.

[1] R. H. Fowler and L. Nordheim, Proc. R. Soc. London, Ser. A **119**, 173 (1928).
[2] R. A. Millikan and C. C. Luritsen, Proc. Natl. Acad. Sci. U.S.A. **14**, 45 (1928).
[3] J. G. Simmons, J. Appl. Phys. **34**, 1793 (1963).
[4] J. G. Simmons, J. Appl. Phys. **34**, 2581 (1963).
[5] A. Schenk and G. Heiser, J. Appl. Phys. **81**, 7900 (1997).
[6] R. G. Forbes, Ultramicroscopy **79**, 11 (1999).
[7] Y. L. Chiou, J. P. Gambino, and M. Mohammad, Solid-State Electron. **45**, 1787 (2001).
[8] E. W. Cowell III, N. Alimardani, C. Knutson, J. F. Conley, D. A. Keszler, B. Gibbons, and J. F. Wager, Adv. Mater. **23**, 74 (2011).
[9] P. Sharma, W. Zhang, K. Amiya, H. Kimura, and A. Inoue, J. Nanosci. Nanotechnol. **5**, 416 (2005).
[10] J. G. Speight, *Lange's Handbook of Chemistry*, 16th ed. (McGraw-Hill, 2005).
[11] E. Bersch, S. Rangan, R. A. Bartynski, E. Garfunkel, and E. Vescovo, Phys. Rev. B **78**, 085114 (2008).
[12] D. Liu, S. J. Clark, and J. Robertson, Appl. Phys. Lett. **96**, 032905 (2010).
[13] M. L. Huang, T. C. Chang, T. D. Lin, J. Kwo, T. B. Wu, and M. Hong, Appl. Phys. Lett. **89**, 012903 (2006).
[14] E. S. Noh, S. E. Ulloa, and H. M. Lee, Phys. Status Solidi B **244**, 4427 (2007).
[15] S. A. Campbell, *Fabrication Engineering at the Micro- and Nanoscale* (Oxford University Press, 2008).
[16] M. V. Fischetti, D. J. DiMaria, L. Dori, J. Batey, E. Tierney, and J. Stasiak, Phys. Rev. B **35**, 4404 (1987).
[17] C. R. Helms and B. E. Deal, *The Physics and Chemistry of SiO_2 and Si-SiO_2 Interface* (Plenum, 1998).
[18] D. J. DiMaria, E. Cartier, and D. Arnold, J. Appl. Phys. **73**, 3367 (1993).
[19] D. Arnold, E. Cartier, and D. J. DiMaria, Phys. Rev. B **49**, 10278 (1994).
[20] E. W. Cowell III, C. C. Knutson, N. A. Kuhta, W. Stickle, D. A. Keszler, and J. F. Wager, Phys. Status Solidi A **209**, 777 (2012).
[21] J. Tregilgas, in *Proceedings of ASM International Advanced Materials and Processes* (2005), p. 46.

[This article is copyrighted as indicated in the article. Reuse of AIP content is subject to the terms at: http://scitation.aip.org/termsconditions. Downloaded to] IP: 128.193.163.187 On: Mon, 10 Mar 2014 19:05:15